THE UNCERTAINTY OF Z_{dr} CALIBRATION TECHNIQUES

J.C. Hubbert,* F. Pratte, M. Dixon and R. Rilling
National Center for Atmospheric Research, Boulder CO

1. INTRODUCTION

Dual polarized radars promise to increase the accuracy of radar rainfall measurements. The copolar differential power measurement, Z_{dr}, as well as the specific differential phase, ϕ_{dp}, contain additional information about the scattering medium that can be used to increase the accuracy of precipitation measurements that are based solely on radar reflectivity. However, to realize this benefit, Z_{dr} should be calibrated to about one tenth of a dB.

NCAR (National Center for Atmospheric Research) has been tasked by the Office and Science and Technology (OS&T) of NWS (National Weather Service) to determine the uncertainty of various methods for the calibration of Z_{dr} using S-Pol, NCAR's S-band polarimetric radar. Three techniques are investigated 1) the vertical pointing (VP) technique, 2) the engineering calibration (EC) technique and 3) the crosspolar power (CP) technique. A primary focus of this investigation is to define the "goodness" of the experimentally determined Z_{dr} biases or calibration factors found from each technique. Estimating Z_{dr} errors is accomplished by 1) repeated experimental trials and 2) from known manufacture specifications and knowledge of RF (radio frequency) measurement test equipment and circuit topology. Uncertainty of measurements is a way to quantify the probability that a measurement (in the present case a calculated calibration factor) lies within some error bounds. Thus, the goal of this this project is to quantify the uncertainty of the estimated Z_{dr} calibration factors determined by each method.

One widely accepted way to calibrate Z_{dr} is to point the radar dish vertically in light rain and measure Z_{dr} while turning the dish 360 degrees. Since raindrops have no preferred orientation (i.e., distributed uniform randomly in the plane of polarization) 360-degree-integrated, intrinsic Z_{dr} is zero dB. Thus, any measured non-zero dB Z_{dr} yields the radar system Z_{dr} offset. This technique works particularly well with radar systems that employ a single copolar receiver so that any receiver drift will not affect the calibration. However if separate horizontal (H) and vertical (V) receivers are employed, the temporal drift of the receivers likely needs to be monitored. Issues with the vertical pointing method are: 1)

*NCAR/EOL, Boulder, Colorado 80307, email: hubbert@ucar.edu

the radar can only be calibrated when there is precipitation over the radar, 2) the precipitation needs to be deep enough so that measurements can be made in the far field and so that measurements are not affected by transmitter transients 3) there is an uncertainty associated with making the VP measurements.

A second way to calibrate Z_{dr} is with an EC approach based on engineering measurements and the following instrument model (Zrnić et al. 2006). The radar transmit and receive paths are divided into "active" and "passive" parts. The gains and losses of the "passive" or "static" parts, i.e. the waveguides and antenna, are measured by using test signals and radiation from the sun. The gain of the active signal path (i.e., receiver chain) is monitored via test signal injection on a continuous basis. Transmit powers are also monitored. By combining the passive and active calibration measurements, the Z_{dr} bias can be estimated. The uncertainty of the EC approach is estimated from a combination of prior experience (Type B evaluation; e.g., manufacturer uncertainty specifications) and on repeated measurements (Type A evaluation) (Taylor and Kuyatt, 1994). Type A evaluations of RF power measurement uncertainty can typically be quite small if the repeated power measurements of a signal with the same measurement equipment is executed by the same technician over a brief time interval, (say minutes). However, such error evaluations do not take into account possible systematic biases A third method for Z_{dr} calibration makes use of the principle of radar reciprocity which states that the two crosspolar members of the radar scattering matrix are equal, i.e, $S_{hv} = S_{vh}$ (Saxon, 1955). Practically, this means that the crosspolar powers measured with a fast alternating H-V polarization transmit radar are equal if the H and V transmit powers are equal. Use of this fact along with passive sun measurements can be used to calibrate Z_{dr} and this technique is termed the crosspolar power (CP) approach for Z_{dr} calibration. The CP method is not based on isotropy of the scatterers (as is the VP method) and has been demonstrated previously with CSU-CHILL radar data (Hubbert et al. 2003). Operationally, the NEXRADs will transmit H and V polarization simultaneously and thus this method will not work directly as it has on S-Pol and CSU-CHILL, i.e., near simultaneous samples of the two crosspolar powers are not available as is the case for fast H and V alternating polarization transmission. However, the average crosspolar powers from stationary ground clutter targets

(e.g., from consecutive PPI surveillance scans at H and V polarization if indexed beams are used) can be measured by employing a slow mechanical switch to alternate H and V transmit polarizations. This is possible since the backscatter cross sections of stationary ground clutter targets are invariant (ground clutter targets such as trees that can move with the wind are exceptions). Such slow switch crosspolar data has not been previously demonstrated but is shown in this paper with S-Pol.

Uncertainty budgets of the three Z_{dr} calibration approaches are compared and discussed. Preliminary results using S-Pol are given that indicate the uncertainty of each method.

2. UNCERTAINTY MEASUREMENT CONCEPTS

Calibration is a measurement process that assigns values to the property of an artifact or to the response of an instrument relative to reference standards or to a designated measurement process. Its purpose is to reduce the bias of the measurement process. There are measurement errors associated with this measurement process. Uncertainty can be defined as an estimate of the expected limits of experimental error. Uncertainty, in general, of measurement arises from incomplete knowledge, control, understanding, and definition of the processes influencing the measurement. Influence effects, such as temperature, humidity, frequency, mechanical stresses, path variations, and mismatches affect the result of measurements. (See http://www.itl.nist.gov/div898/handbook/index.htm for more detailed treatment of calibration and uncertainty).

Uncertainty can be categorized as either Type A or Type B. Type A uncertainty is represented by the standard deviation of a set of measurements and is primarily quantified by repetition under controlled test conditions (sometimes referred to as under statistical control). Type B uncertainty can also be represented by the standard deviation of an assumed Normal Distribution but is not quantified through measurement. It is quantified through manufacture specifications and other prior knowledge.

Errors can also be categorized (modeled) as systematic or random. Systematic measurement errors bias the mean of a measurement data set, i.e., increasing the number of measurements and averaging will not reduce systematic errors as it will random errors. One way to detect and correct for systematic errors is to use a calibration standard, if one exists. Typically, subtle systematic errors are the most difficult to detect, model and quantify. If all systematic errors are eliminated, the remaining fluctuations in a measurement data set are considered random measurement errors and can be quantified by calculation of the standard deviation of the data set. The random errors are usually considered Gaussian distributed but this

assumption should be examined for each data set. The systematic errors, however, can also be modeled as random Gaussian distributed and included in an uncertainty budget.

An uncertainty specification is incomplete without a confidence interval (Taylor and Kuyatt 1994). The confidence interval used in this report is 2σ or two standard deviations. This is sometimes referred to as 2σ coverage. The 2σ coverage standard is used in this report since this is the coverage value typically used by manufactures of RF devices. It also seems reasonable that meteorologist/hydrologists would like to use Z_{dr} measurements that are calibrated to within 0.1 dB with 95% confidence (i.e., 2σ coverage). In fact, the NEXRAD Technical Advisory Committee recently recommended (in March 2007) that Z_{dr} be calibrated to within 0.1 dB with 95% confidence (i.e., 2σ coverage).

The measurements presented in this report are typically expressed as

$$E = M \pm \delta \tag{1}$$

where E is the quantity estimated, M is the measurement (or mean of measurements) and δ represents the uncertainty of the measurement with 2σ coverage. The desired Z_{dr} calibration goal can be expressed as

$$Z_{dr}^{cal} = Z_{dr}^{m} + Z_{dr}^{bias} \pm \delta \tag{2}$$

where Z_{dr}^{cal} is the corrected or calibrated Z_{dr}, Z_{dr}^{m} is the measured Z_{dr} estimated from radar data, Z_{dr}^{bias} is the Z_{dr} bias calculated via one of the calibration techniques and δ is the 2σ uncertainty of the bias estimate. Note that other possible biases to the Z_{dr}^{cal} estimate that are external to the radar, such as differential propagation attenuation, are not considered here.

Use of automated test equipment, described later, for calibration measurements permits more complete decomposition of Z_{dr} uncertainty and will reduce human error and variance in measurement due to repeated connects and disconnects. Such equipment and methodology will improve the understanding of the measurement process and the quantification of the uncertainty. Whether or not the Z_{dr} calibration measurement uncertainty can be reduced to less than 0.1 dB is currently being evaluated using S-Pol as a test bed for NEXRAD.

3. AUTOMATED TEST EQUIPMENT (ATE)

Mechanical processes and procedures such as attaching and re-attaching cables, couplers and meters introduce variability to the EC approach. To reduce these effects, Automatic Test Equipment (ATE) has now been built into S-Pol to measure test point signals, inject test

signals and monitor environmental variables such as temperature along the signal path using fixed cable attachments and electronic switches. Figure 1 shows a block diagram of S-Pol. The green box shows the ATE with its multiple input and output lines marked in yellow. The shown yellow connectors (small circles) are connected to the other Test Points also marked in yellow. The S-Pol system has two parallel processors: 1) the VIRAQ (developed by NCAR) and 2) the SIGMET RVP8.

The transmit RF signal (red box) goes through a power distribution network which provides for 1) fast alternating H and V polarization transmission (pulse to pulse) via a fast mechanical switch 2) simultaneous H and V transmission via a power divider 3) H only transmission and 4) V only transmission. The transmit signal(s) pass through the circulators, Test Point 3, rotary joints, Test Point 2 and then to the antenna/dish. The received signal passes back through to the circulators and then the LNAs. Physically, the transmitter, the circulators, the LNAs and the remaining receiver and processor circuits are all located in the S-Pol "transmitter trailer". After demodulation to IF (intermediate frequency), the signals pass through a switch shown in blue. The switch can direct the IF signals to either IF amplifier #1 (called copolar amp.) or IF amplifier #2 (called crosspolar amp.). When operating in fast alternating H and V transmission mode, the switch is typically used to direct the copolar signals to the same IF amplifier so that any temporal variation in the IF amplifier and remaining sections of the receiver/processor will affect both copolar signals equally. This is done to reduce the variance of Z_{dr} measurements. Thus, S-Pol has four separate receiver paths to calibrate: 1) H signal to IF amp #1, 2) H signal to IF amp #2, 3) V signal to IF amp #1, and 4) V signal to IF amp #2. Test Point 4 yields the digitized in phase and quadrature (I and Q) samples (see http://www.eol.ucar.edu/rsf/spol/spol.html for a description of S-Pol).

Inside the ATE is a control computer, wideband power meter, signal generator, noise sources, attenuators and an RF switching matrix all of quality necessary to achieve overall 0.1 dB measurement uncertainty. Appropriate control connections are established between the ATE and the digital receiver, transmitter, and antenna pedestal. The ATE records the process measurements and the radar scans of the sun. Over a period of months a data base will be created so that a statistical analysis of the calibration measurements will ultimately lead to an estimate of the uncertainty of the EC Z_{dr} method. Data from the VP approach will be used with ATE data to evaluate the EC approach. An EC method is routinely employed at both CSU-CHILL and S-Pol, however, it typically has been found that a systematic Z_{dr} bias persists which must be corrected using vertical pointing data in light rain.

4. ENGINEERING CALIBRATION APPROACH

The EC method breaks the calibration task into two parts: 1) measurement of the gain of the *static* portion of the of the signal path via injected signals, passive solar radiation and power meters, and 2) monitoring of the *dynamic* portion of the received signal path via the injection of test pulses. The static portions of the signal path are the waveguides and antenna. It is hypothesized that these signals can be measured accurately enough to calibrate Z_{dr} to within 0.1 dB uncertainty. The active or time varying portion of the receiver chain runs from the circulators through the I&Q digital samples. The active portion of the receiver chain likely needs to be monitored on a volume scan to volume scan basis using test pulses. The active portion of the Z_{dr} calibration applies to all the calibration techniques. The principle behind all of the calibration techniques is to measure the differential path losses 1) from the transmitter out through the antenna and 2) from outside the antenna back through to the received I and Q samples. Note that the path from the circulators through the antenna is common to both transmit and receive paths. It can be shown that the following calibration equation accounts for the entire electrical transmit and receive paths. The Z_{dr} calibration equation is,

$$Z_{dr}^{bias} = \Delta(1,2)_{pulse} + 2\Delta(S,4)_{noise} - \Delta(2,4)_{noise}. \quad (3)$$

where the terms are in dB. The $\Delta(1,2)_{pulse}$ term is a measurement of the differential path loss from the transmitter to measurement plane 2. Physically, the radar transmit pulses are monitored at measurement plane 1 and RF power measurements are made at plane 2 via a waveguide coupler. The term $\Delta(S,4)_{noise}$ determines the differential gain from outside the antenna to the I and Q samples using the sun as an unpolarized RF source (i.e., the H and V power from the sun are equal, a very good assumption (Tapping 2001)). The $\Delta(2,4)_{noise}$ term is measured by injecting noise at measurement plane 2 and measuring the resulting differential power at measurement plane 4 via the I and Q samples. In this way, the system Z_{dr}^{bias} is measured. Thus, to determine the uncertainty of this Z_{dr} bias estimate is tantamount to determining the Z_{dr} bias of each term on the right hand side of Eq. (3) in conjunction with each other.

The Type A uncertainty of a particular repeated RF power measurement (i.e., simply repeating an RF power measurement while the circuit topology and components are constant) can be very low, perhaps on the order of a hundredth of a dB; however, as explained above, there are systematic errors (typically Type B) that must be taken into consideration: for example the uncertainty of the waveguide coupling factor, impedance mismatches and other systematic biases. These types of errors cannot

be reduced with repeated trials and averaging.

4.1 *An Engineering Calibration Uncertainty Estimate*

In this section the uncertainties of making waveguide power measurements are discussed and applied to the uncertainty budget of Eq. (3). Shown in Fig. 3 is a picture of an experimental power measurement from inside the transmitter trailer at S-Pol. The H and V waveguide are seen at the top of the picture. The waveguide couplers are blue and connected to the waveguide couplers can be seen the attenuator, power sensor and power meter. For this setup, the attenuator would be disconnected from one waveguide coupler and attached to the other waveguide coupler to complete the differential power measurements. This power measurement capability is now handled by the ATE automatically. Figure 4 shows a block diagram for a differential power measurement. In this setup (modeled after the ATE) a switch is used to select either the H or V waveguide for measurement. Shown also are circles that indicate some of the various uncertainties that affect power measurement. Table 1 gives a description of the uncertainties and typical values (2σ coverage, for high quality, well calibrated test equipment).

Assume that there are RF signals in the waveguides. To make a single power measurement (say from the H-waveguide), a waveguide tap is used to extract power from the waveguide, the signal passes through an attenuator, is converted to to a DC voltage which is then measured by the power meter. Each of the uncertainty factors along the electrical path, shown in Fig. 3 and numerically given in Table 1, are added in quadrature to ascertain the total uncertainty (quadrature is the square root of the sum of squares). When adding uncertainties in quadrature, the uncertainties are assumed independent. If it is suspected that the uncertainties are not independent and their relationship is unknown, then the uncertainties should be simply added which would yield a higher uncertainty than the quadrature addition (Taylor 1997). The estimated uncertainty of a single power measurement can be expressed

$$
\begin{aligned}
U_m^H \;=\; & f\big(U_c^H,\, U_{w,c}^H,\, U_{w,s}^H,\, U_s,\, U_{s,a},\, U_a, \\
& U_{a,p},\, U_p,\, U_m\big).
\end{aligned} \tag{4}
$$

Using the values given in Table 1, the 2σ uncertainty is 0.195 dB.

For differential power measurements, some of the uncertainties will cancel, e.g., the uncertainties due to the attenuator, power sensor and power meter are common to both the H and V measurements and thus cancel in the ratio of H and V power measurement. The uncertainty of the differential waveguide power measurement can be expressed,

$$
U_m^D = f\left(U_c^H,\, U_{w,c}^H,\, U_{w,s}^H,\, U_c^V,\, U_{w,c}^V,\, U_{w,s}^V\right) \tag{5}
$$

where U_m^D is the differential power measurement uncertainty. Again, the uncertainties are assumed independent and are combined in quadrature to yield a total uncertainty of 0.183 dB.

This uncertainty can be regarded as an estimate of the uncertainty of the $\Delta(1,2)$ term in the EC calibration Eq. (3) where the transmit pulse power is measured at test plane 2 (the uncertainty of the power of the H and V transmit pulses is not included). If the same waveguide couplers are used to inject signals for the purposed of determining the $\Delta(2,4)$, more of these uncertainty terms in Eq. (5) will cancel when calculating the overall uncertainty of Eq. (3). Specifically, the uncertainty of the waveguide coupling factor, U_c, will cancel.

- *An important observation is that the coupling factor for a waveguide coupler is bi-directional or reciprocal where as the associated impedance mismatch factors are not.*

Thus, if a signal is injected via the switch by a generator (gn) as shown in Fig. 4 for the purpose of measuring $\Delta(2,4)$, when calculating the uncertainty of Eq. (3), the waveguide coupler uncertainty factor will cancel; however, the uncertainties due to impedance mismatches will not cancel due to the non reciprocity of these factors. Thus, the direction of the RF signal is accounted for with the superscripts "inj" for inject a signal into the waveguide while "out" denotes that a signal is extracted from the waveguide. The total uncertainty of Eq. (3) can be expressed

$$
\begin{aligned}
U_m^T \;=\; & f\big(U_{w,c}^{H_{inj}},\, U_{w,s}^{H_{inj}},\, U_{w,c}^{V_{inj}},\, U_{w,s}^{V_{inj}},\, U_{w,c}^{H_{out}}, \\
& U_{w,s}^{H_{out}},\, U_{w,c}^{V_{out}},\, U_{w,s}^{V_{out}},\, U_s,\, U_{gn}, \\
& U_{g,s},\, U_{sun},\, U_{tx}\big)
\end{aligned} \tag{6}
$$

where the "inj" is associated with the impedance mismatch at the waveguide coupler interfaces when signal is being injected into the waveguide, the "out" is associated with the impedance mismatch at the waveguide coupler interfaces when signal is being sampled from the waveguide. As can be seen from Eq. (6), the uncertainty of making a Z_{dr} bias estimate via Eq. (3) is due in large part to impedance mismatches. Other uncertainties are U_{gn} the signal generator, U_s switch jitter, U_{sun} sun variability and processing procedures (0.05 dB), and U_{tx} the power injection uncertainty for the measurement $\Delta(1,2)$ (0.05dB). The impedance mismatches are quite significant and the 2σ uncertainty estimate due to just just the 8 waveguide impedance

mismatch terms is 0.186 dB (i.e., adding the 8 individual uncertainty estimates of 0.06 dB in quadrature). Adding the rest of the uncertainties yields $U_m^T = 0.192\,dB$. The uncertainties used are taken from Table 1 where we assume $U_{w,c}^{H_{inj}} = U_{w,c}^{H_{out}} = U_{w,c}^{H}$ and similarly for the other impedance mismatches.

a. *Impedance mismatch factors*

For each interface a connection of some sort needs to be made and for each connection there will exist an impedance mismatch that will give rise to unknown reflected signal that will alter the power measurement. Each mismatch alteration is itself deterministic and may be corrected if the relevant scattering parameters of the junction are known, however this correction is complex.

Though vector power measurements are deterministic, scalar power measurements cannot be considered such because of the unknown signal reflection coefficients at the connections. The error components for this evaluation tend to be small compared to the error limits of test equipment and procedures. This is termed a low "accuracy ratio". The uncertainty performance of the calibration measurement process must be better than the measurement uncertainty of the instrument being calibrated. That is the "accuracy ratio".

The reflection coefficient (Γ) is a complex number closely related to scattering parameters S_{11} and S_{22} of two-port junctions. Return loss in decibels and voltage standing wave ratio (VSWR), cited in component specifications, is related to the magnitude of reflection coefficient $|\Gamma|$ as follows

$$RL_{dB} = 20\log(|\Gamma|)$$
$$VSWR = (1 + |\Gamma|)/(1 - |\Gamma|) \quad (7)$$
$$|\Gamma| = (1 - VSWR)/(VSWR + 1)$$

For evaluation of mismatch we employ the following power transfer equations

$$P_{ds} = M_{gs}P_{ag} \quad (8)$$

$$P_{dl} = M_{gl}P_{ag} \quad (9)$$

where P_{ds} is the power delivered to the power sensor, P_{dl} is the power delivered to the load, if different from the sensor, M_{gs} and M_{gl} are the mismatch factors, and P_{ag} is the available power from the generator. M_{gs} and M_{gl} range between 0 and 1 depending on how well the match conditions for maximum power transfer are satisfied (Kearns and Beatty 1967).

$$Mgs = (1 - |\Gamma_g|^2)(1 - |\Gamma_s|^2)/(|1 - \Gamma_g\Gamma_s|^2) \quad (10)$$

In Table 2, the magnitudes of typical impedance mismatch uncertainties from (10) are presented, corresponding to return losses of approximately -30 dB, -20 dB, and -15 dB typically found for microwave radar system components.

Table 2 shows the magnitude of mismatch errors that occur at a power measurement interface when a load with excellent, good, or fair match is connected to a generator with good match. It is evident that controlling the VSWR of each junction to a maximum of 1.2, but preferably better under various measurement conditions, is essential to reach the goal of 0.1dB expanded uncertainty. Mu + and Mu- are the uncertainties at worst-case phase angles. The column labeled $U|\Gamma_l|$ is the calculated standard uncertainty under the assumption of a uniform distribution of reflection coefficient Γload and phase; the column Const$|\Gamma_l|$ assumes that the reflection coefficient Γload is as specified but again with uniform phase on each side of the interface (Agilent Technol. 2001).

The reader is reminded that though the right hand columns represent likely uncertainty at each measurement junction, there will be several such measurements that contribute to the combined uncertainty.

Mismatch errors do not possess normal distributions and have been further evaluated with Monte Carlo simulations. Results are shown in Figs. 6 and 7 corresponding to columns U$|\Gamma_l||$ and Const$|\Gamma_l|$ of Table 2. The distributions distributions are not Gaussian a show the potential of faily large errors even for well matched components. Either the impedance match of components must be carefully controlled for these scalar power measurements, or the more difficult vector power measurements may be used.

Most microwave measurement texts and articles devote a substantial percentage to treatment of ways to mitigate mismatch effects for precise power measurement. On a macro level many of the explicit and implicit assumptions are tantamount to assuming reciprocity, that the implicit impedance matches are "stationary" and reciprocal to a degree that is better than measurable (say 0.01 dB). It is assumed for now without verification that intermodulation and harmonic content are well below the signals of interest. This is subverted in at least two cases that we can think of: (1) the circulator will not have the same reflection coefficient when in transmit mode as when receiving. However for now we assume that the circulator is nearly ideal and its maximum return loss is -20 dB under various conditions; (2) the return loss of the antenna system will depend on antenna position by virtue of "wow" in the rotary joints and variable radome seam scattering. Again we assume nearly ideal components and a maximum return loss of -20 dB under various conditions.

5. THE CROSSPOLAR POWER APPROACH

The CP method has been successfully applied to the

CSU-CHILL radar data to calibrate Z_{dr} (Hubbert et al. 2003). The technique uses the property of radar reciprocity (Saxon 1955) which states that the off diagonal terms of the radar scattering matrix, S_{hv}, S_{vh}, are equal (Bringi and Chandrasekar 2001). Using this fact the Z_{dr} calibration equation can be derived:

$$Z_{dr}^{cal} = Z_{dr}^m S^2 \frac{\overline{P_{xv}}}{\overline{P_{xh}}} \qquad (11)$$

where Z_{dr}^{cal} is calibrated Z_{dr}, Z_{dr}^m is measured Z_{dr}, S is the ratio of the V and H power from sun measurements, and $\overline{P_{xh}}$, $\overline{P_{xv}}$ are the average crosspolar powers for transmit H and transmit V polarization, respectively. The crosspolar powers may be averaged over a few rays or an entire volume of radar data. Both precipitation as well as ground clutter targets may be used. If precipitation targets are used, fast alternating H and V transmit polarizations must be used. The CP Z_{dr} calibration approach is like the VP technique in that neither require waveguide couplers, signal sources nor power meters and thus the associated uncertainty related to such RF measurements is eliminated.

S-Pol employs a copolar and crosspolar receiver design in contrast to H and V receivers. This is done to reduce the variance and drift of the Z_{dr} measurement but this also slightly changes the Z_{dr} calibration equation to:

$$Z_{dr}^{cal} = Z_{dr}^m S_1 S_2 \frac{\overline{P_{xv}}}{\overline{P_{xh}}} \qquad (12)$$

where S_1 is the ratio of V-copolar to H-copolar sun radiation and S_2 is the ratio of V crosspolar to H crosspolar sun radiation (See Hubbert et al. 2003 for details).

6. EXPERIMENTAL RESULTS

In this section we present experimental results that are indicative of the uncertainty of the measurements that are required for the three Z_{dr} calibration techniques. Data come from both the RVP8 and VIRAQ processors. In the following analysis we assume that all systematic errors are negligible and thus we are estimating the uncertainty due to random errors. Any systematic error should be evident when the Z_{dr} biases calculated from the EC, CP and VP methods are compared.

6.1 Sun Measurement Statistics

Both the EC and CP calibration techniques require sun measurements. The sun radiation at S-Band is assumed unpolarized (Tapping 2001) and thus the H and V powers are equal. During high sun spot activity, there can be

circularly polarized radiation also (Tapping 2001). However, circularly polarized radiation will also split equally into H and V polarized components.

The following data is processed by VIRAQ. On 8 August 2006, 13 consecutive "box scans" of the sun were made. The azimuth scan with the highest power point is selected and then the azimuth scan before and after are also selected. Five beams are then selected from each scan centered on the beam with the highest power. Gates 150 through 950 are used and with 32 samples per gate, this gives a total number of I&Q samples of about 384,000. These samples are averaged for each box scan in order to estimate S_1 and S_2 that are required for the crosspolar power calibration technique. The calculated $S_1 S_2$ numbers are (linear scale)

0.7760 0.7789 0.7854 0.7773 0.7843 0.7713 0.7795
0.7745 0.7812 0.7767 0.7744 0.7801 0.7732

The mean is 0.7780 with a standard deviation of 0.0042. The standard deviation is 0.023 dB and the 2σ uncertainty of the 0.7780 mean estimate is 0.0130 dB. This indicates that the uncertainty of the $S_1 S_2$ product over a short time interval (about 0.5 hours) is well within the 0.1 dB uncertainty desired for NEXRAD Z_{dr} measurements.

From 14 June to 24 August, 309 sun box scans were made and the mean ratios S_1 and S_2 were calculated. Figures 8 and 9 show histograms of these 309 values (linear scale). The means are 0.883 and 0.886, respectively, while the standard deviations are 0.005 and 0.006, respectively. This yields a uncertainty (2σ) of 0.049 dB for S_1 and 0.058 for S_2 *over the entire 72 day measurement period*. Figure 10 shows the histogram of the product $S_1 S_2$ and the mean is 0.781 with a standard deviation of 0.0091. The uncertainty is 0.10 dB. These uncertainty values are likely dominated by variations in the gains of the LNAs since they are the only active component in the differential path. Figure 11 shows the time series of the $S_1 S_2$ values. The plot indicates that although the variance of the $S_1 S_2$ product is small, it should be monitored frequently in order to to keep the Z_{dr} calibration uncertainty under 0.1 dB.

6.2 Sun Integration Techniques and Antenna Patterns

The above is a Type A evaluation of the uncertainty of sun power ratio measurements. There are likely systematic errors present that are not evident from Type A evaluations. Important in the above assessment of uncertainty is the used integration technique. Typically the sun is scanned with one tenth degree elevation steps at about one degree per second rate. Obviously, the location of the one tenth of a degree separated elevation angle cuts through the sun will vary from one sun scan to another

and this could affect the calculation of of the S_1S_2 ratio needed for Z_{dr} calibration.

To reduce this possible error source, a more sophisticated integration technique is investigated next. The following data is processed by RVP8. To reduce the sun integration errors, sun data points are first interpolated to a uniform rectangular $0.1° \times 0.1°$ grid. In order to determine the location of the sun center (considered the maximum power point), data along each of the vertical and horizontal grid lines are fitted to a Gaussian shaped curve and the location of the horizontal and vertical maximums of the Gaussian shaped curves are considered as the center of the sun. Note that the sun's center may not fall on on one of the grid points. The data is then integrated over different annuli corresponding to different radii. Fig. 12 shows the ratio S_1S_2 for sun scan data gathered from 26 July 2006 to 10 October 2007. The annuli of integration have $0.25°$ and $1.25°$ diameters. As can be seen the curves agree fairly well with the variance of the $0.25°$ curve being greater than the variance of the $1.25°$ curve. To further examine the effect of integrating the sun scans over various annuli, consider Table 3. Given in Table 3 are the means (linear units) and the fractional standard deviations (FSTD) (dB) calculated from 303 sun scans. The interpolation scheme combined either two or three sun scans to obtain one interpolated data set. There are 18 interpolated data sets that used two scans scans and 89 data sets that used three sun scans for a total of 107 interpolated sun scan data sets. Table 3 shows that the means of the sun scan data sets are nearly independent of the annulus of integration. The FSTD are also very similar with the lowest value achieved for an annulus of $1.25°$.

To gain additional insight, such grided solar scan data can be used to construct "pseudo" antenna patterns. After compensating for the sun's movement and correcting for the radar elevation angle, the data can be used to construct "pseudo" antenna patterns in the sense that the distributed solar source is used instead of a point source. To estimate the true antenna pattern one would need to deconvolve the sun illumination pattern. The sun could be approximated as having uniform brightness over a disk that subtends about $0.53°$ though the sun behavior is considerably more complex. For a more full assessment of the sun's radiation see Tapping (2001), Kraus (1986) and Jursa (1985). Figures 13, 14 and 15 show the H, V and the H to V ratio antenna patterns. The H and V "pseudo" patterns are well matched across their $1°$ beam width but there is some difference outside these limits. To obtain non-biased Z_{dr} measurements of precipitation, the H and V antenna patterns must be well matched across their main lobes (Hubbert et al., Appendix C, 1998). Figure 16 shows the correlation between the measured H and V antenna patterns. Since the sun's radiation is unpolarized (there can be exceptions to this during high solar activity when the radiation can be circularly polarized) the expected correlation between the two patterns is 0. Figure 16 shows that the correlation over the center of the H and V antenna patterns is very low but there are four lobes of higher correlation. These four lobes are caused by the depolarization of the electric field by the four antenna reflector support struts.

To gain further insight on the S_1S_2 ratio, the S_1S_2 ratio "antenna pattern" can be also calculated and is shown in Fig. 17. As can be seen the S_1S_2 pattern is fairly symmetric so that when integrating over the various annuli, the mean value does not change much, as show in Table 3.

Finally, we compare the standard deviation of the mean sun scan values for the two integration techniques shown in Fig. 11 and Fig. 12(the RVP8 $1.25°$ curve). Using data only from 26 July 2006 to 31 October 2007, the FSTDs are found to be about 0.05 dB for the data of Fig. 11 and 0.02 dB for the $1.25°$ data of Fig. 12. This then indicates that the griding of the sun scan data and integrating over an annulus does indeed reduce the standard deviation of the S_1S_2 estimates and reduces some of the possible systematic errors associated with the sun integration technique and procedure.

The more sophisticated sun data integration procedure first grids the data taking into account the sun's movement and the radar elevation angle and thus the region over which the sun scan data is integrated is much better controlled. Therefore, better sun statistics (less variance) are produced and the presence of possible systematic errors is reduced.

6.3 *Vertical Pointing Measurements*

Vertical pointing measurements in rain have an intrinsic Z_{dr} of 0 dB when data is averaged over a $360°$ rotation of the radar dish. A measured non-zero value is considered the system Z_{dr} bias. To evaluate the uncertainty of the VP Z_{dr} bias estimate, six consecutive iZ_{dr} bias measurements were made while S-Pol was vertically pointing in light rain on 31 August 2006 using RVP8. Each measurement results from integrating measured Z_{dr} over one $360°$ antenna revolution and over the range between 2 and 9 km above the radar for data with SNR> 30 dB. The calculated numbers are (in dB):

0.7267 0.7232 0.7210 0.7112 0.6929 0.6726

The mean is 0.712 dB and the standard deviation is 0.019 dB. The 2σ uncertainty of the mean estimate is 0.007 dB. Note that this is a Type A assessment of the random component of the VP Z_{dr} calibration but it does not include possible systematic errors due to the data processing technique.

6.4 *Crosspolar Power Data*

In addition to the sun measurements, the CP technique for Z_{dr} calibration requires the measurement of the mean crosspolar power ratio, $\overline{P_{xv}/P_{xh}}$. On 31 August 2006 several volume scans of storms cells were made by S-Pol in fast alternating H and V mode using RVP8. The number of samples per gate was 64 and the scan rate was $12°\text{s}^{-1}$. Data were averaged over 14 separate PPI scans at elevation angles above $2°$. Clutter returns are filtered out by requiring the absolute radial velocity to exceed $2\,\text{ms}^{-1}$. Clutter returns can also be used since clutter targets should also be reciprocal scatterers and thus can be used for the Z_{dr} calibrations. This is considered later. The power ratios of $\overline{P_{xv}/P_{xh}}$ are, in dB:

-0.312 -0.335 -0.326 -0.341 -0.347 -0.357 -0.347
-0.263 -0.276 -0.304 -0.337 -0.319 -0.343 -0.319

The mean is -0.323 dB and the fractional standard deviation is .026 dB so that the 2σ uncertainty is 0.046 dB for the individual mean estimates. However, the mean estimate of -0.323 dB is more reliable and the 2σ uncertainty is 0.014 dB.

As mentioned before, the NEXRAD dual polarization system will use simultaneous H and V transmission and reception and thus, near simultaneous samples of H and V crosspolar returns will not be available. However, if two slow waveguide switches are used then the NEXRADs will be able to measure both crosspolar powers. One technique for the evaluation of $\overline{P_{xv}/P_{xh}}$ is to alternate between only H and only V transmission on a PPI to PPI basis. If the beams are indexed, crosspolar powers from the same resolution volumes (but from different PPI scans) can be paired and used for the CP calibration. On 18 October 2006 this measurement technique was tested using RVP8 data. Elevation scan data was collected in fast alternating transmit H and V mode, followed shortly by H-only transmit, and then V-only transmit modes. The crosspolar power ratios were calculated from both sets of data. For 22 H and V PPI pairs, the mean crosspolar power ratio is $\overline{P_{xv}/P_{xh}} = 0.373$ dB with a 2σ uncertainty of 0.032 dB. Similarly, for the fast alternating mode, the mean $\overline{P_{xv}/P_{xh}} = 0.404$ dB and the 2σ uncertainty is 0.002 dB. The uncertainty of $\overline{P_{xv}/P_{xh}}$ for the fast alternating method is much lower than that for the alternate H and V PPI method; however, these results suggest that the cross polarization approach is amenable to NEXRAD.

6.5 *Comparison of Calubration Techniques*

The Z_{dr} calibration factor or bias of the S-Pol system should be the same whether using the vertical pointing (VP), the crosspolar power or engineering techniques. The Z_{dr} bias calculated above from VP data is 0.712 dB$\pm$0.019 dB. The Z_{dr} bias can also be calculated via the CP technique using Eq.(12) from sun measurements and crosspolar power measurements, also gathered on 31 August 2006. $S_1 S_2$ was found to be -1.051 dB$\pm$0.013 dB while the crosspolar power ratio was -0.323 dB$\pm$0.014 dB. This yields a Z_{dr} bias of $(-0.323) - (-1.051) = 0.728$ dB$\pm$0.027 dB which is in excellent agreement with the VP bias estimate 0.712 dB$\pm$0.019 dB. Both of these uncertainties are derived from Type A evaluations. The is likely other Type B errors that we have neglected for both techniques. For the VP we estimate a Type B uncertainty of 0.05 dB. For the CP technique, we estimate an uncertainty of 0.05 dB for both the crosspolar power ratio $\overline{P_{xv}/P_{xh}}$ and the sun ratio measurement $S_1 S_2$. This then changes the VP bias estimate to 0.712 dB$\pm$0.053 dB and the the CP estimate to 0.728 dB$\pm$0.075 dB. Both 2σ uncertainties are still under the 0.1 dB requirement. The results from the EC approach indicate Z_{dr} measurement bias is 0.80 dB with a total uncertainty of about 0.25 dB (other uncertainties are are included in this estimate that were not included in Section 4.1 above. The EC bias number of 0.80 dB was estimated from data taken over several days so that a direct comparison of the EC bias to the CP and VP biases is not warranted. The uncertainty estimate of the EC bias, 0.25 dB, however, more importantly indicates that the EC Z_{dr} bias may not be estimated to within the 0.1 dB requirement. More data sets need to be gathered to confirm these numbers.

7. CONCLUSIONS

NCAR is conducting an experiment for OS&T of NOAA/NWS to evaluate Z_{dr} calibration techniques for the WSR-88Ds using S-Pol, NCAR's S-band polarimetric radar. Three techniques for Z_{dr} calibration were investigated: 1) vertical pointing data in light rain, 2) engineering calibration technique and 3) the crosspolar power technique. Measurement and analyses were performed in order to quantify the uncertainty of the estimated calibration numbers and the measurement procedures that yield such uncertainty. The uncertainty of measurements can be separated into two categories: 1) systematic and 2) random. Vertical pointing (VP) measurements in light rain are widely regarded as the most accepted way to calibrate Z_{dr} and such measurements were used to truth other Z_{dr} calibration measurements. Several sets of vertical pointing data were gathered over the the summer of 2006 and analysis showed that the Type A uncertainty of the vertical point Z_{dr} calibration was on the order of 0.01 dB. Again, this is an evaluation of the *random measurement*

errors and possible systematic biases may be present, e.g. due to data processing. A main objective of this Z_{dr} calibration experiment is to determine the uncertainty associated with the EC Z_{dr} calibration technique. The uncertainty of the EC technique was established via both Type A and Type B uncertainty evaluations. These results are preliminary and the uncertainty estimate should improve as the measurement methods are improved. The Z_{dr} bias calculated for the EC technique was measured to be about 0.80 dB with an uncertainty estimated to be about 0.25 dB (2 σ coverage). The 0.25 dB uncertainty number is dominated by impedance mismatches.

Evaluation of sun measurements impacts both the engineering calibration technique (EC) as well as the crosspolar power technique (CP). The sun's radiation (at S-band) can be considered unpolarized and thus the power of the sun is equally divided between horizontal (H) and vertical (V) polarizations. Sun flairs can create polarized radiation but is typically circular polarization which also provides equal powers between the H and V channels. Thus, the sun's radiation is an excellent RF source for the evaluation of the differential gain of a radar's H and V receive channels. For the S-Pol system that uses a switch at the IF stage to create copolar and crosspolar receivers, there are two sun power ratios required for the CP calibration technique, namely S_1 and S_2. It is the product of these two ratios that appears in the calibration equation Eq.(12). Analysis of data sets of the $S_1 S_2$ product gathered over about 0.5 hour yield a fractional uncertainty of 0.0041 dB. From 14 June to 24 August 309 solar box scans were made and a long term analysis of S_1 and S_2 from this data set yielded an uncertainty of 0.049 dB (2σ).

Measurements with S-Pol thus far show excellent agreement between the Z_{dr} bias found via VP measurements and the CP techniques (biases of 0.712 dB and 0.728 dB, respectively). For the experimental data used here, both techniques yielded uncertainties within the desired uncertainty limit of 0.1 dB. Additionally, it was shown that the crosspolar power technique can successfully be employed on radar systems that achieve dual polarization measurement via simultaneous transmission of H and V polarizations as NEXRAD will do. In this case, slow waveguide switches were used to gather alternate PPIs of transmit only H and transmit only V data. Using indexed beams, the transmit H and transmit V crosspolar powers from the alternate PPIs were equated. This can done for ground clutter since the backscatter cross sections of stationary ground clutter targets is invariant. These results indicate that the crosspolar technique could be used with NEXRAD type radars.

Further and improved evaluation of the Z_{dr} calibration techniques will be accomplished with the Automated Test Equipment (ATE) which was recently completed. Data sets where all three Z_{dr} calibration techniques can be executed in close temporal proximity (with a half hour) are needed.

References

Agilent Technologies, 2001: Fundamentals of rf and microwave power measurements. Technical report, Agilent Technologies, application Note 64-1C.

Bringi, V. and V. Chandrasekar, 2001: *Polarimetric Doppler Weather Radar*. Cambridge Univ. Press, Cambridge, UK.

Doviak, R.J., V.N. Bringi, A. Ryzhkov, A. Zahrai, and D.S. Zrnić, 2000: Polarimetric upgrades to operational WSR-88D radars. *J. Atmos. Oceanic Technol.*, **17**, 257–278.

Hubbert, J.C., V.N. Bringi and D. Brunkow, 2003: Studies of the polarimetric covariance matrix: Part I: Calibration methodology. *J. Atmos. and Oceanic Technol.*, **20**, 696–706.

Jursa, A.S. (Editor) , 1985: *Handbook of Geophysics and the Space Environment*. National Technical Information Service, iSpringfield , VA, 4 edition.

Kearn, D. and R. Beatty, 1967: *Basic Theory of Waveguide Junctions and Introductory Microwave Analysis*. Pergamom Press.

Kraus, J.D. , 1986: *Radio Astronomy,*. Cygnus-Quasar Books, 2nd edition.

Saxon, D.S., 1955: Tensor scattering matrix for the electromagnetic field. *Phys. Rev.*, **100**, 1771–1775.

Tapping, K. : 2001, Antenna calibration using the 10.7 cm solar flux. *Radar Polarimetry for geoscience applications*, P. Smith, ed., American Meteorological Society, http://cdserver.ametsoc.org/cd/010430_1/RADCAL_Links_2_Presentations.html.

Taylor, B.N., and C.E. Kuyatt, 1994: Guidelines for evaluating and expressing the uncertainty of NIST measurements results. Technical report, US Dept. of Comm. National Institute of Standards and Tech., note 1297.

Taylor, J.R., 1997: *An Introduction to Error Analysis*. University Science Books, Sausalito, CA.

Zrnić, D.S., V.M. Melnikov, and J.K. Carter, 2006: Calibrating differential reflectivity on the WSR-88D. *J. Atmos. and Ocean. Tech.*, **23**, 944–951.
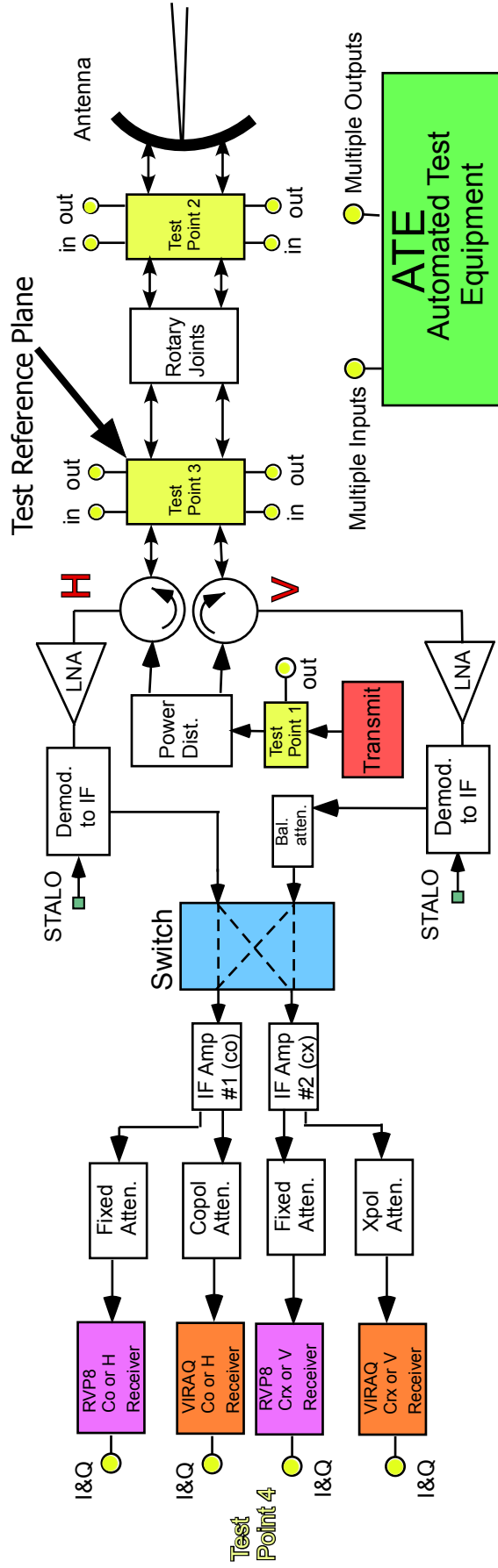
Figure 1: *A block diagram of S-Pol showing the Automated Test Equipment.*
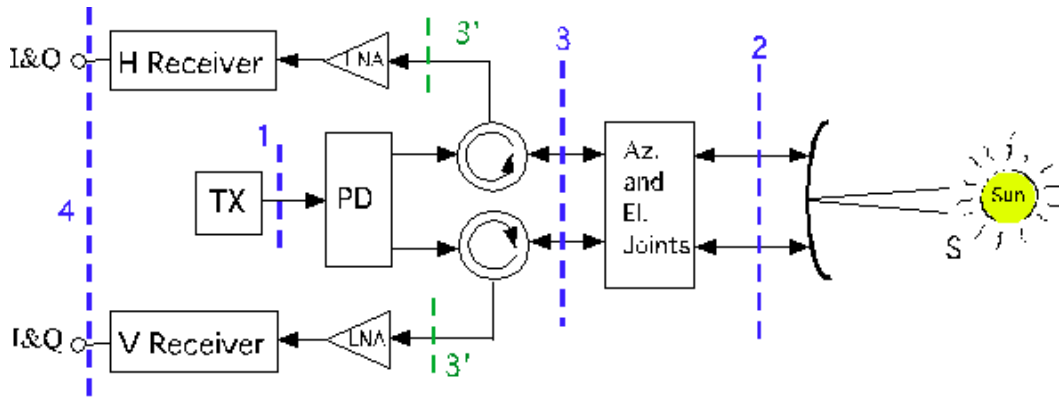
Figure 2: *A block diagram of a radar system for the EC method.*

Uncertainty	Description	value (dB)
U_s	Waveguide coupling factor	0.1
U_s	Switch	0.01
U_a	Attenuator	0.08
U_p	Power sensor (RF to DC)	0.09
U_m	Power meter	0.05
$U_{w,c}$	Impedance mismatch between waveguide coupler and waveguide	0.06
$U_{c,s}$	Impedance mismatch between waveguide coupler and switch	0.06
$U_{s,a}$	Impedance mismatch between switch and attenuator	0.06
$U_{g,s}$	Impedance mismatch between generator and switch	0.06
U_{gn}	generator noise	0.02
U_{gn}	Sun source & processing	0.05

Table 1: *A list of 2σ uncertainties for the differential power measurement shown in Fig. 4 .*

						Model A	Model B
						$\mathbf{U}\|\Gamma_l\|$	$\mathbf{Const}\|\Gamma_l\|$
$\|\Gamma$ load$\|$	VSWR	RL load	RL load (dB)	Mu- (dB)	Mu+ (dB)	u(Mu) (dB)	u(Mu)
0.024	1.050	0.001	-32.256	-0.0052	0.0052	0.002	0.004
0.091	1.200	0.008	-20.828	-0.0721	0.0715	0.025	0.050
0.200	1.500	0.040	-13.979	-0.3546	0.3407	0.121	0.239

Table 2: *Relationship between reflection parameters and impedance mismatches selected to represent excellent, good, and average match conditions of a sensor connected to a generator having a return loss of -20 dB. See text for explanation of mismatch quantities shown in the four right-hand columns.*

Annuli	$0.25°$	$0.50°$	$0.75°$	$1.00°$	$1.25°$	$1.50°$	$1.75°$	$2.00°$
Mean (lin)	0.7762	0.7756	0.7755	0.7754	0.7754	0.7752	0.7752	0.7753
FSTD (dB)	0.0313	0.0261	0.0217	0.0214	0.0197	0.0212	0.0229	0.0277

Table 3: *The mean (linear) and the fractional standard deviation (FSTD)(dB) of sun scan data gathered from 26 July 2006 to 20 March 2007 for various annuli of integration centered on the sun maximum power.*
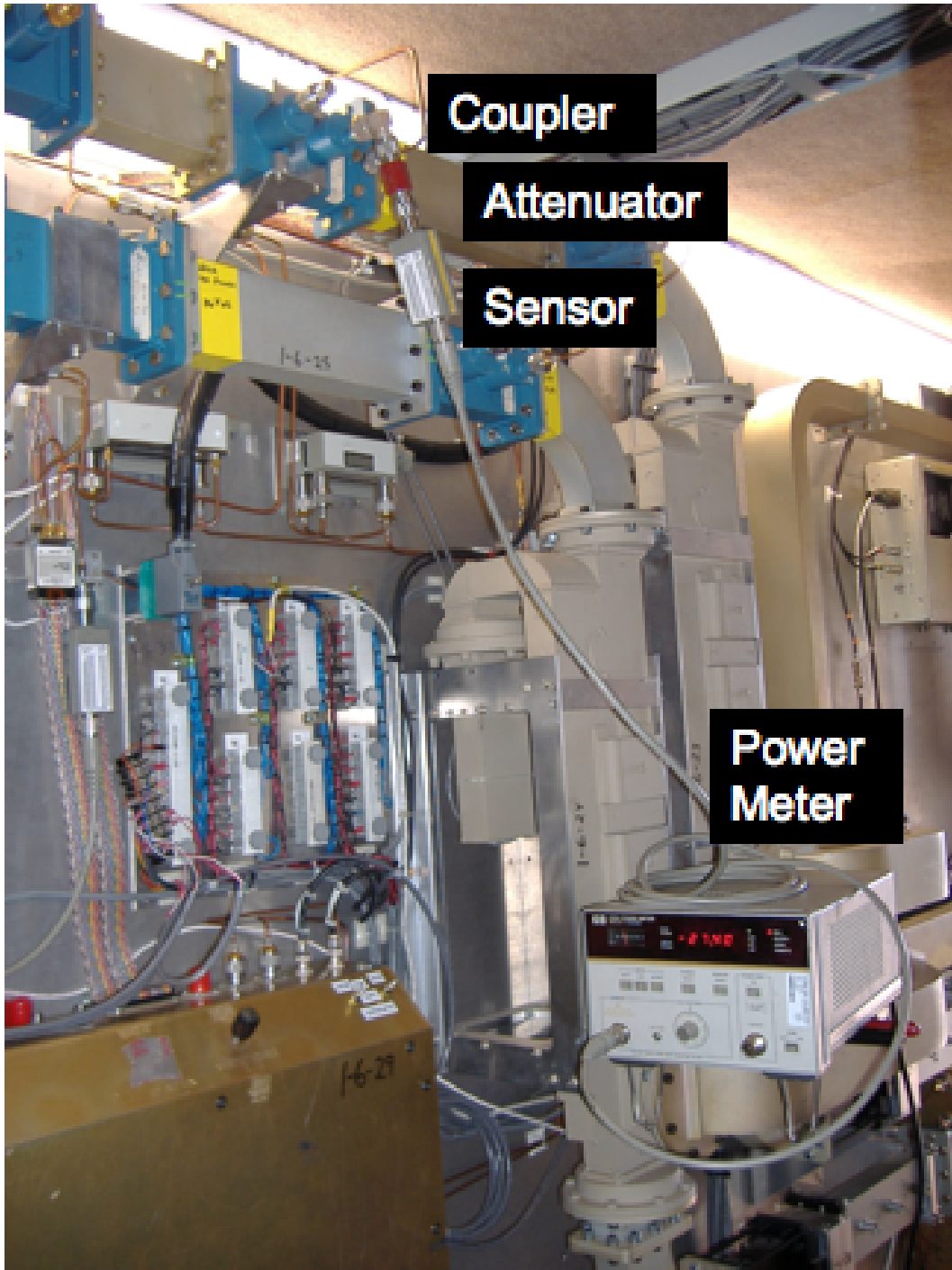
Figure 3: *A picture of a power measurement made inside the S-Pol transmitter trailer.*
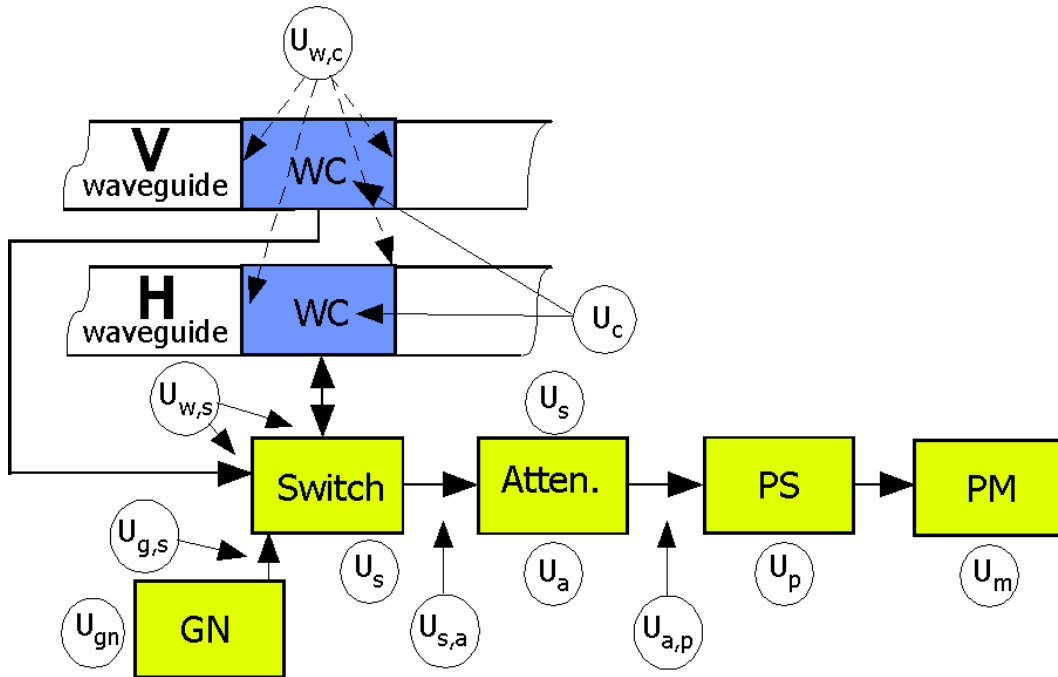
Figure 4: *A block diagram of a differential waveguide power measurement. "WC" is waveguide coupler, "Atten." is an attenuator, "PS" is a power sensor, "PM" is a power meter and "GN" is a generator. The circles represent the various uncertainties. The double subscripted uncertainties are various impedance mismatches between the devices. A list of the uncertainties with definitions is given in Table 1*
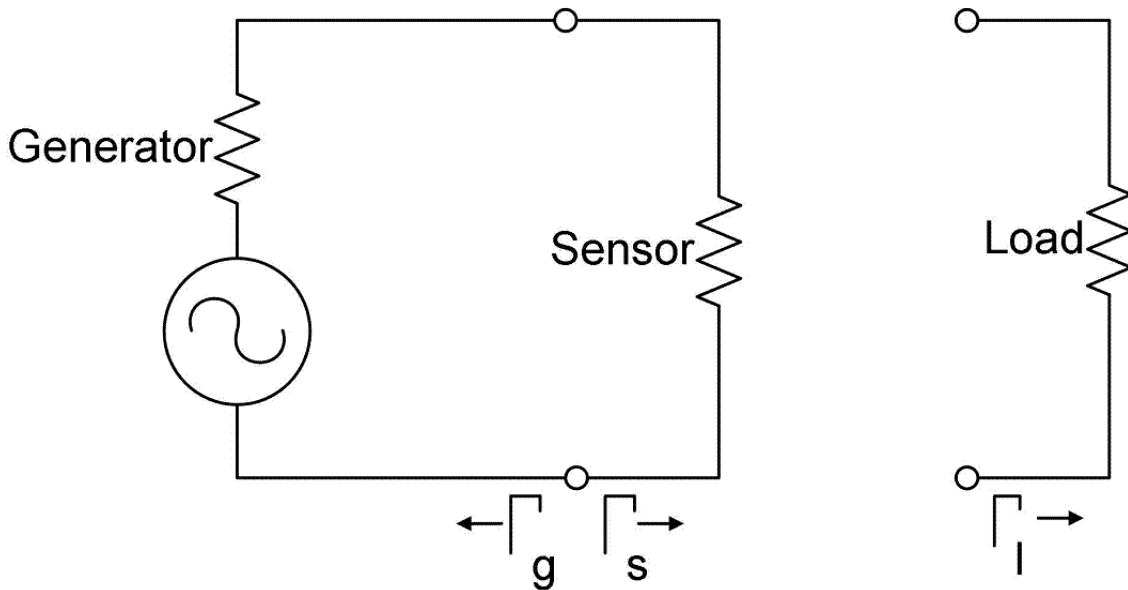

Figure 5: *Basic circuit for mismatch error evaluation of power delivered to a sensor and to a directly substituted load. A two-port microwave junction, such as an attenuator or a cable, may be placed between the generator and load.*
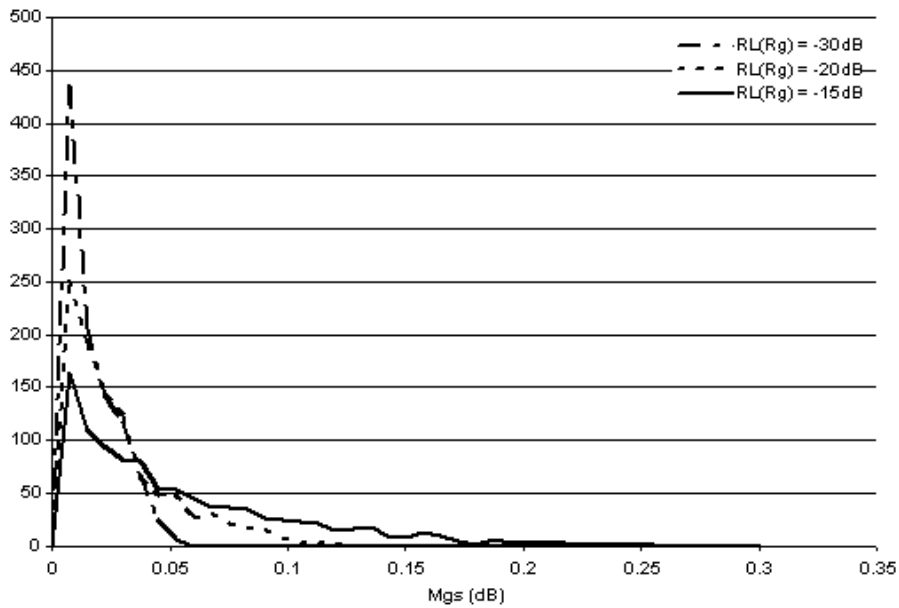
Figure 6: *Histogram of simulated (Monte Carlo, 1000 trials) mismatch factors based on a sensor return loss uniformly distributed up to -20 dB and generator return loss uniformly distributed up to -30 dB, -20 dB, and -15 dB, and uniformly distributed phases.*
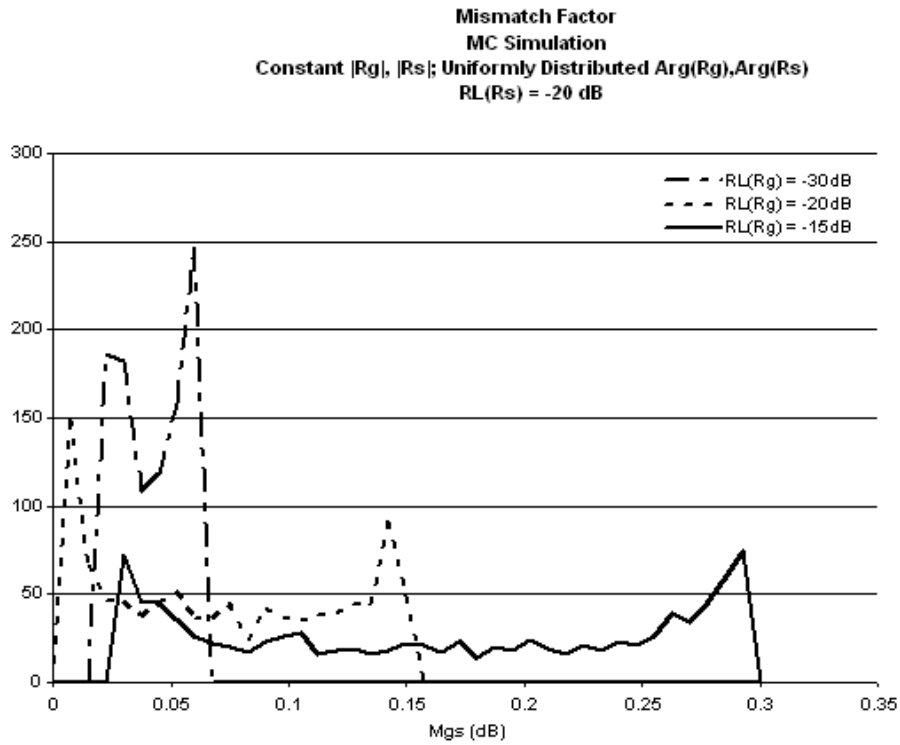
Figure 7: *Histogram of simulated (Monte Carlo, 1000 trials) mismatch factors based on a sensor return loss of a constant -20 dB and generator return loss constant at -30 dB, -20 dB, and -15 dB, and uniformly distributed phases.*
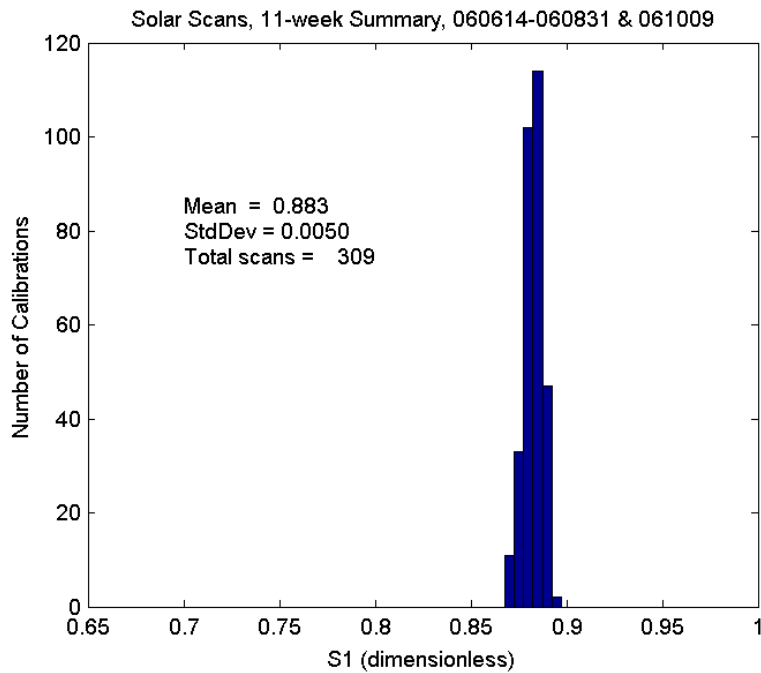
Figure 8: *Histogram of 309 S_1 ratio measurements.*
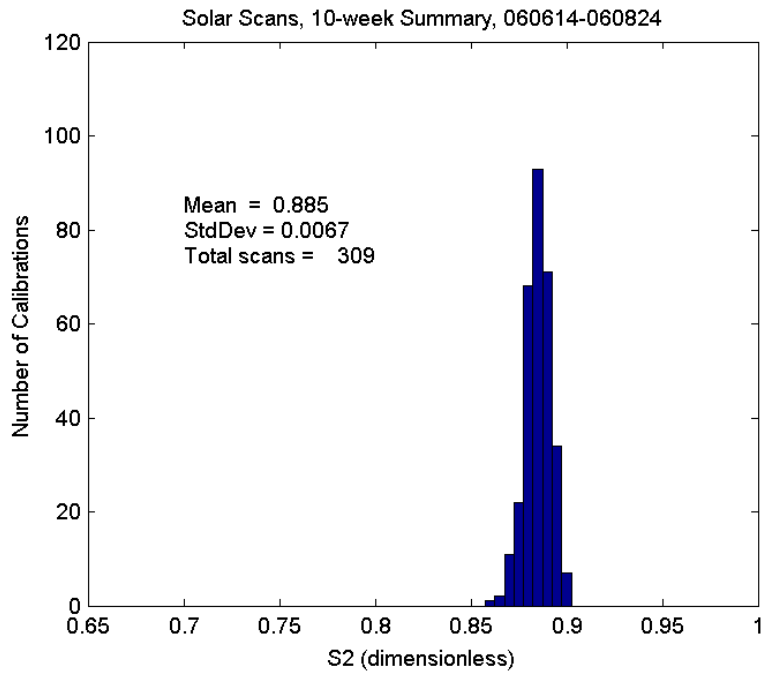
Figure 9: *Histogram of 309 S_2 ratio measurements.*
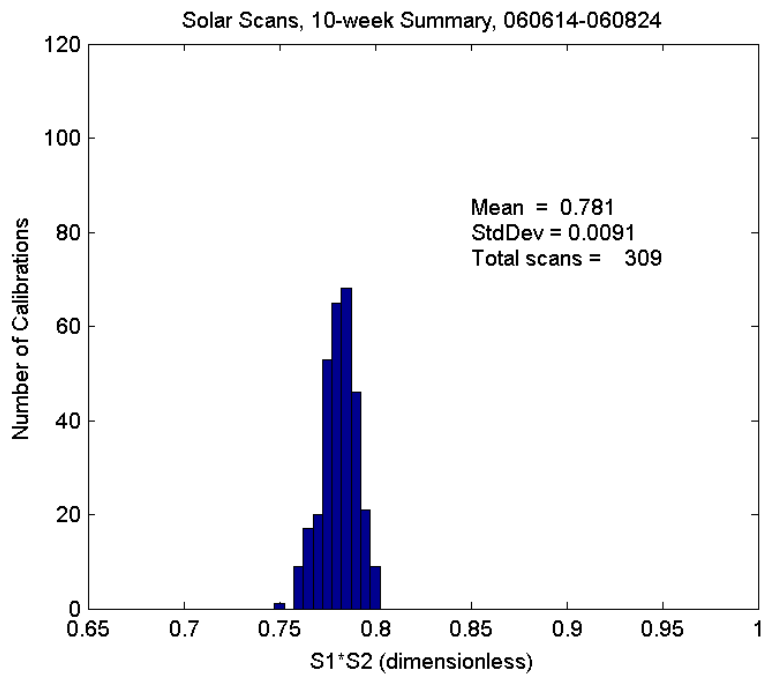
Figure 10: *Histogram of 309 S_1S_2 ratio measurements (linear scale).*
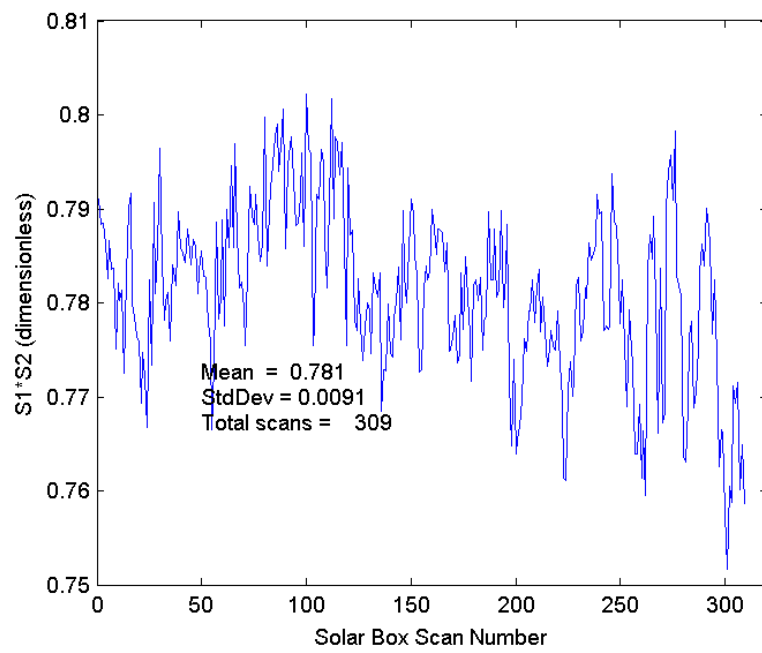
Figure 11: *Time series of the 309 $S_1 S_2$ ratio measurements (linear scale).*
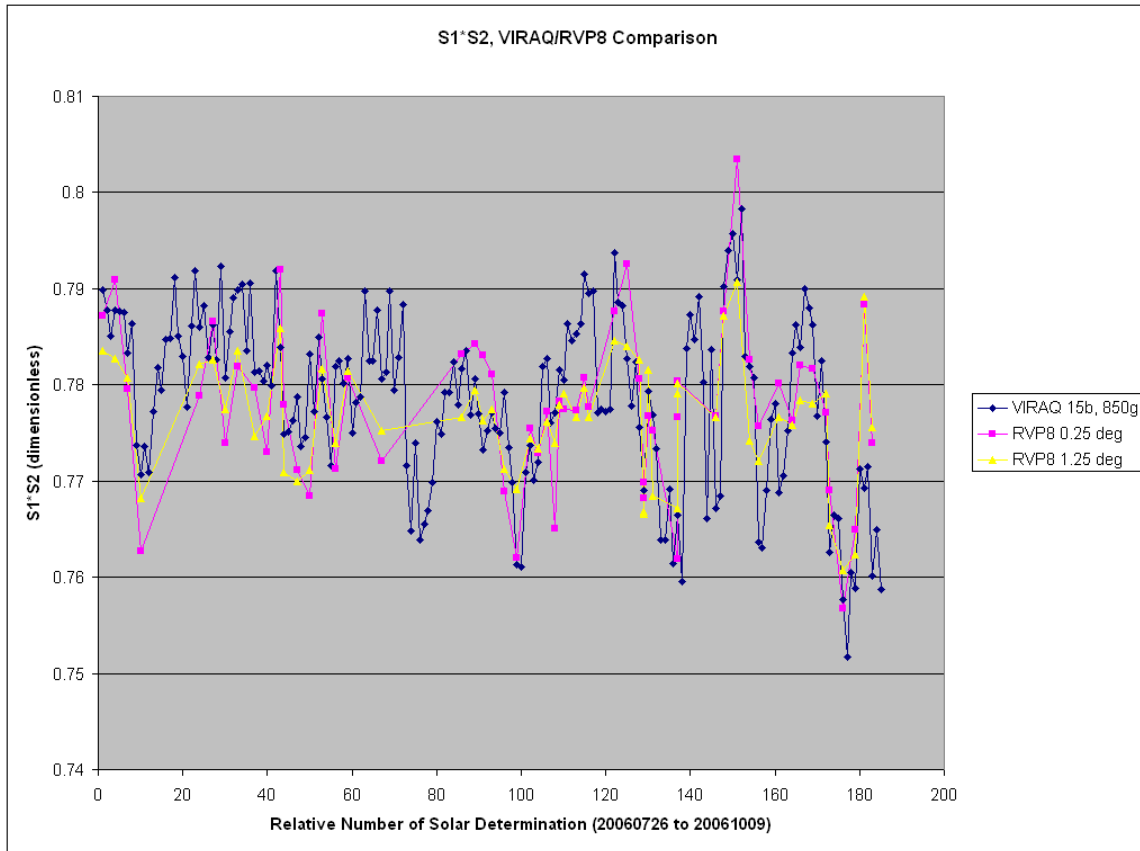
Figure 12: *Time series of mean values of $S_1 S_2$ calculated from from sun scan data gathered from July 2006 through October 2006.*
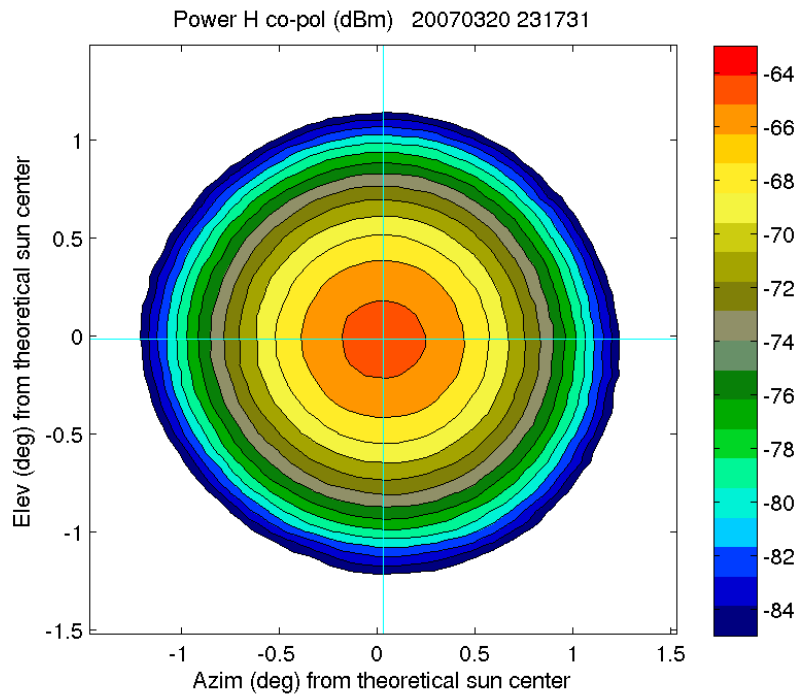
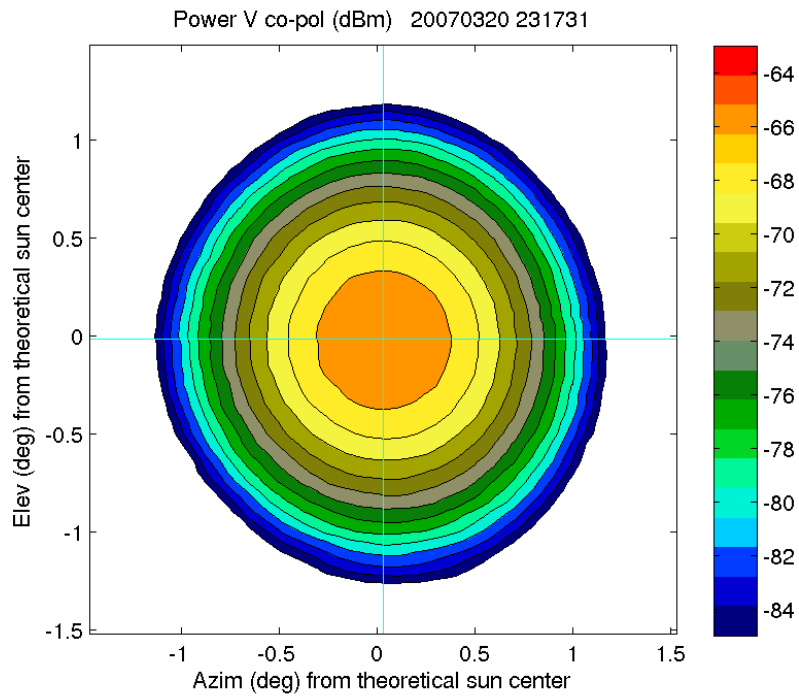Figure 13: *Pseudo H antenna pattern from sun measurements*

Figure 14: *Pseudo V antenna pattern from sun measurements. Note the vertical elongation along the vertical axis.*
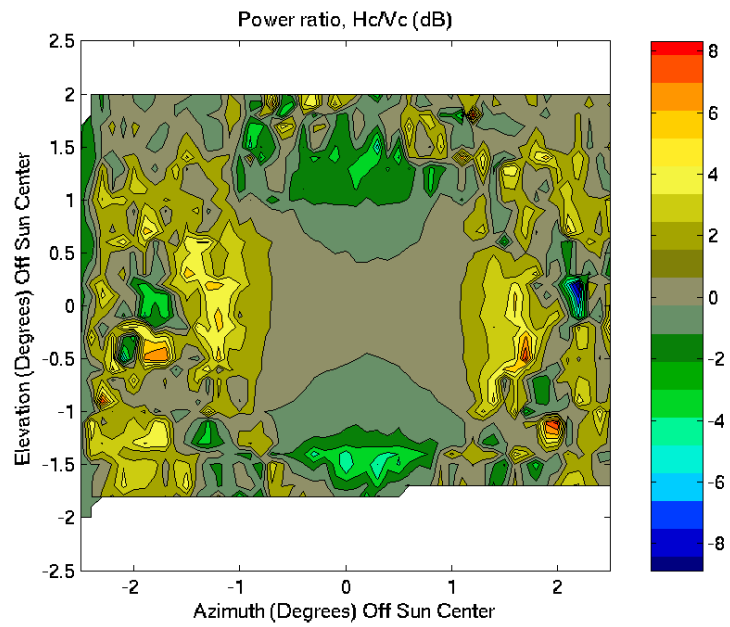
Figure 15: *The ratio of H and V antenna patterns from Figs. 13 and 14.*
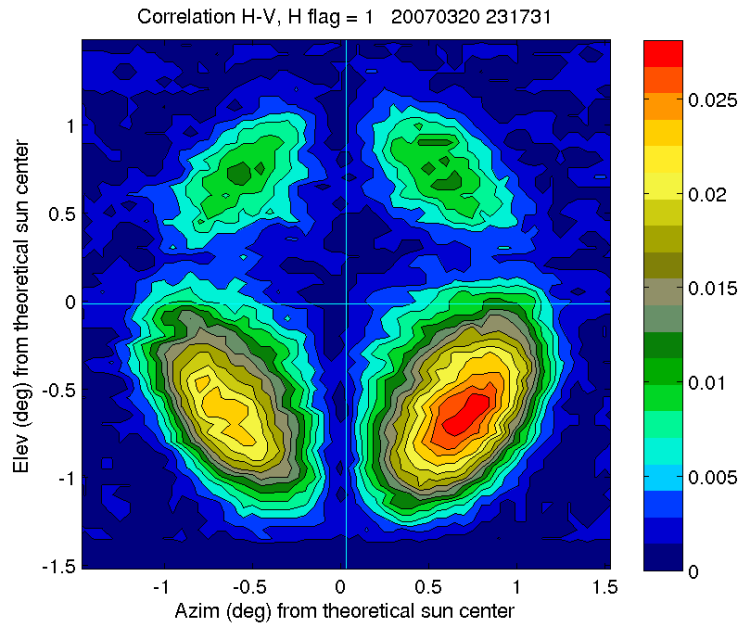

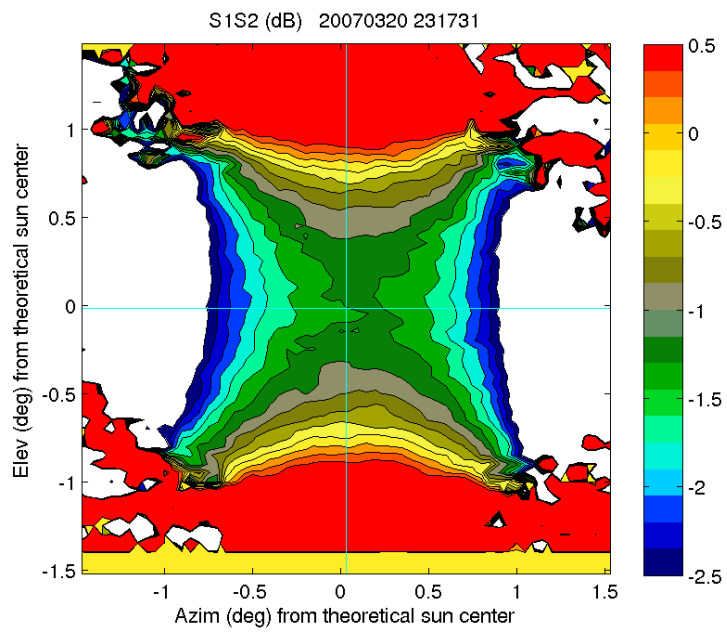Figure 16: *Correlation between the H and V antenna patterns of Figs. 13 and 14.*

Figure 17: *The ratio S_1S_2 antenna pattern from corresponding to Figs. 13 and 14.*